13th International Symposium on Turbulence and Shear Flow Phenomena (TSFP13)
Montreal, Canada, June 25–28, 2024

EXPERIMENTAL INVESTIGATION OF ACOUSTIC SCATTERING BY A TURBULENT SHEAR LAYER

Francesco Scarano*, Vincent Clair, Antonio Pereira, Edouard Salze
Lab. de Mécanique des Fluides et d'Acoustique (LMFA), Ecole Centrale de Lyon
36 Av. Guy de Collongue, 69130 Ecully, France
*fr.scarano@gmail.com

Joannes Chambon
MicrodB
Écully, France

ABSTRACT

An experiment is conducted to link the scattering of acoustic waves by a turbulent field in a shear layer with the turbulent features of the shear layer. Microphones measurements highlighted a spectral broadening around the carrier tone with the formation of two sidelobes. The application of SPOD to the particle image velocimetry (PIV) results obtained in the shear layer reveals that the most energetic mode of the spanwise velocity component has a peak at a frequency that corresponds to the side-lobes of the acoustic spectrum. Synced PIV and acoustic measurements demonstrate a correlation between the time delay/anticipation of the acoustic wave traversing the shear layer and the instantaneous spanwise velocity coherent motion.

1 INTRODUCTION

An acoustic wave that impinges a shear layer is convected by the uniform flow, refracted by the mean velocity gradient and scattered by the turbulent field. Due to the scattering, a source tone measured far-field, after the acoustic wave has traversed the shear layer, does not emerge as a narrow peak in the energy spectrum. The spectrum exhibits a broadening and the tone energy is redistributed into a broadband field centred around the carrier tone, with the presence of two side-bands colloquially called "haystacks" (McAlpine *et al.* (2013)).

Examples of industrial context where haystacking is of interest are the propagation of a tone radiated from the exhausted nozzle through a turbulent shear layer (Ewert *et al.* (2009)), the acoustic propagation through the atmospheric boundary layer and far-field acoustic measurements conducted in an open jet wind tunnel. In the last case the model to study is usually located in the potential region of the jet; the acoustic field that propagates from the model impinges and traverses the shear layer that develops on the sides of the nozzle. The acoustic waves are scattered causing a broadening of the spectral content and an attenuation of the tone energy (Sijtsma *et al.* (2014); Kroeber *et al.* (2013)). Having further insight into the physics of the haystacking is of primary importance for acoustic imaging techniques that experience error caused by signal coherence loss due to the turbulence field (Sijtsma (2008)).

Lighthill (1953) carried out the first theoretical studies on the scattering of acoustic field by turbulence, then Kraichnan (1953) focused on the modification of the spectrum by isotropic turbulence. Candel *et al.* (1976*a*) developed an analytical models to predict the haystacking and more recently Clair & Gabard (2018) focused on the scattering produced by a single eddy or a turbulent shear layer with constant width. According to Candel *et al.* (1976*b*) the broadening of the spectrum and the two sidelobes can be expressed as

$$|\Delta f| \cong \frac{U_c}{\ell} \tag{1}$$

where Δf is the frequency shift of the side-bands with respect to the carrier frequency, f_0; $U_c = U_0/2$ is the convective velocity and ℓ is a characteristic scale of the large eddies, sometimes called scattering lengthscale, that is found to scale with the vorticity thickness δ_ω (Candel *et al.* (1976*b*); Kroeber *et al.* (2013); Sijtsma *et al.* (2014); McAlpine *et al.* (2013)). In the works by Candel *et al.* (1975, 1976*b*) it is suggested that spectral broadening is dominated by Doppler like effects and, according to Clair & Gabard (2018), the haystacking is due to a combination of a scattering of sound due to the refraction of waves that propagate through a vortical structure and a double Doppler shift, one linked with the motion of the turbulent structure relative to the source and the other linked with the relative motion between the turbulent structure and the observer. Sijtsma *et al.* (2014) proposed an alternative explanation for the haystacking that links the formation of sidelobes with the time delay variation due to the turbulent shear layer. In their work they derived an analytical expression that evaluates the energy decay of the carrier tone and the formation of sidelobes as a function of shear layer properties: the convective velocity, the thickness of the shear layer, the source frequency and the spanwise velocity fluctuations.

Despite several hypothesis have been drawn to model the haystacking, and several studies have been conducted to theoretically or experimentally investigate the scattering of acoustic waves by a turbulent field, some of them cited above, doubts remains on which turbulence feature in the shear layer interacts with acoustic transmission and leads to a modification of the acoustic spectrum. In the current paper, we aim to gain further insight into the physics of haystacking by investigating the

link between the shear layer properties and the generation of sidebands in the acoustic spectrum. For the first time in the literature we explore the subject relying on synced microphones and time resolved particle image velocimetry (PIV) surveys. Spectral proper orthogonal decomposition will be employed to better highlight the turbulent features in the shear layer that interact with the acoustic waves.

2 EXPERIMENTAL SETUP

The experiments are conducted in the anechoic open jet wind tunnel of the Laboratoire de Mécanique des Fluides et d'Acoustique (LMFA) at the École Centrale de Lyon. The jet is equipped with a nozzle having a contraction ratio of 1.25 ending with a square exit section that measures 0.5 m side. The anechoic room where the jet enters measures 730 m^3. The maximum speed achievable with the current contraction ratio is around 80 m/s, the choice, that imposes a limit to the maximum speed, is dictated by the need of having a sufficiently extended potential core region where to place the acoustic source. The tests are conducted at a free-stream velocity of $U_0 = 35, 55$ and 75 m/s (Mach number 0.10, 0.16 and 0.22).

The acoustic source consists in a speaker embedded on one side of a NACA-shaped support and located along the centreline of the jet. The acoustic field is generated by a compression chamber connected to the speaker and located beneath the support. The source is connected to three microphones inside the NACA-casing that are used as a reference. The amplitude of the acoustic source is chosen in order to be clearly distinguished from the broadband noise generated by the jet and the trailing edge noise of the source support. The source vertical position is at $z = 0$, that corresponds to half of the vertical side of the side of the nozzle, where the shear layer can be considered plane, see figure 1. The source streamwise positions is x_s =500 mm downstream the exit of the jet. Three frequencies are tested $8, 12, 16$ kHz.

A SoundCam antenna is used to perform the acoustic measurements, it consists of five branches connected to a central portion. 84 MEMS microphones are located along the branches and the centre of the antenna. A branch of the antenna is aligned with the flow along the streamwise direction; the branch is located at the same z height of the source (lays in the same xy plane of the source). Care is given in aligning one microphone of the branch with the source streamwise position in order to have $x_m = x_s$. Each acoustic measurement is performed at 51.2 kHz for 60 s. The antenna is located at two distances with respect to the source, $Y_r = 1500$ mm (nominal condition) and $Y_r = 579$ mm (closer condition). The distances reported are related to the microphone aligned with the source.

Planar PIV is employed to characterise the shear layer at 35 and 55 m/s (the 75 m/s case has been characterised using hot wire anemometry but the aerodynamic results are not shown here for brevity). The measurement plane is horizontal (xy) in the plane containing the source and the branch of the antenna aligned with the source. The PIV plane is centred with the streamwise location of the source, x_s =500 mm. Two smoke generators are employed, one to seed the core of the jet and the second to seed the anechoic chamber in order to have sufficient particle density in the shear layer. To keep the particle image size between 2 and 4 pixels and reduce peak-locking effects the particle images are slightly defocused (Michaelis *et al.*, 2016). A double pulsed Continuum Mesa PIV laser is employed to illuminate the particles. The acquisition frequency is set to 5 kHz. A Phantom VEO1310L 12 bits CMOS camera equipped with a 60 mm f/2.8 Micro Nikkor lens is used as imaging tool. Lavision DAVIS 10.2 is used for the calibration, synchronisation,laser control and image acquisition. Each run consists in 4900 image pairs for a duration of 0.98 s. Almost 20 runs are acquired in order to have a sufficient convergence of the statistics allowing to resolve the largest flow features. For each of the three source frequency tested and the two free-stream velocities, at least one run is synced with the antenna measurements. The samples are processed using the 2D2C cross-correlation PIV algorithm of DAVIS 10.2. The interrogation window size was iteratively changed passing from 64×64 pixel to 8×8 with an overlap of 50%; this leads to a vector spacing of $\Delta x = \Delta y$ =0.665 mm and 34200 vectors. The field of view (FOV) is 158 mm $\times$ 212 mm ($2.2\delta_\omega \times 1.6\delta_\omega$, where δ_ω is the vorticity thickness).

3 RESULTS

3.1 Shear layer characterisation

The shear layer characterisation is depicted in figure 2. According to Bell & Mehta (1990), the self-similarity of the shear layer is assured by the linear growth of the vorticity thickness, $\delta_\omega(x) = \frac{U_0}{\left(\frac{\partial U(x)}{\partial y}\right)_{\max}}$, the collapse of the statistics when plotted using reduced coordinates (figure 2), where x is the streamwise location and σ is the spreading parameter (Görtler (1942)) and the plateau of the peaks of the statistics in the streamwise direction (not shown here for brevity).

3.2 Power spectral density of acoustic signal and bicoherence

The power spectral density (PSD) of the acoustic signal obtained with the microphone of the antenna located at the same streamwise location of the source ($x_m = x_s$) are reported in figure 3. The spectra are computed using the Welch algorithm with 94 segments, a window size of 2^{15} samples and 50% overlap. The spectra are then centred with the source frequency and normalised by the peak energy following Sijtsma *et al.* (2014). The effect of changing the tone frequency for a fixed free-stream velocity (figure 3 (a)) evidences that the energy associated to the sidelobes increases when the frequency increases because the acoustic wavelength decreases and the interaction with the shear layer is stronger (an higher amount of energy is scattered). When increasing the free-stream velocity for a fixed carrier frequency the side-lobes shift towards larger frequencies (the frequency shifts are approximately equal to 50, 80 and 100 Hz) as predicted by Candel *et al.* (1976*b*) (equation 1). When the source location is shifted downstream the vorticity thickness is larger, the scattering is stronger and the frequency of the sidelobes decreases.

As done by Bennaceur *et al.* (2016) on LES data, we performed the bicoherence on the pressure signal following the formulation reported by Kim & Powers (1979)

$$\mathrm{Bic}^2(x_i, f_1, f_2) = \frac{|\langle \hat{F}(x_i, f_1)\hat{G}(x_i, f_2)\hat{H}^*(x_i, f_1 + f_2)\rangle_b|^2}{\langle |\hat{F}(x_i, f_1)\hat{G}(x_i, f_2)|^2 |\hat{H}(x_i, f_1 \pm f_2)|^2\rangle_b} \quad (2)$$

where F, G and H are three signal f_1 and f_2 are two frequencies and $\langle\rangle_b$ is the average of the blocs in which the signals is divided. In the current case the bicoherence spectrum is computed on one microphone that corresponds to the $x_m = x_s$, namely ($F = G = H$) in the case where the microphones antenna is located closer to the shear layer, so that the aerodynamic low frequency content of the shear layer is captured in the pressure signal as depicted in figure 4 (a). The bicoherence represents the non-linear interaction between the frequencies

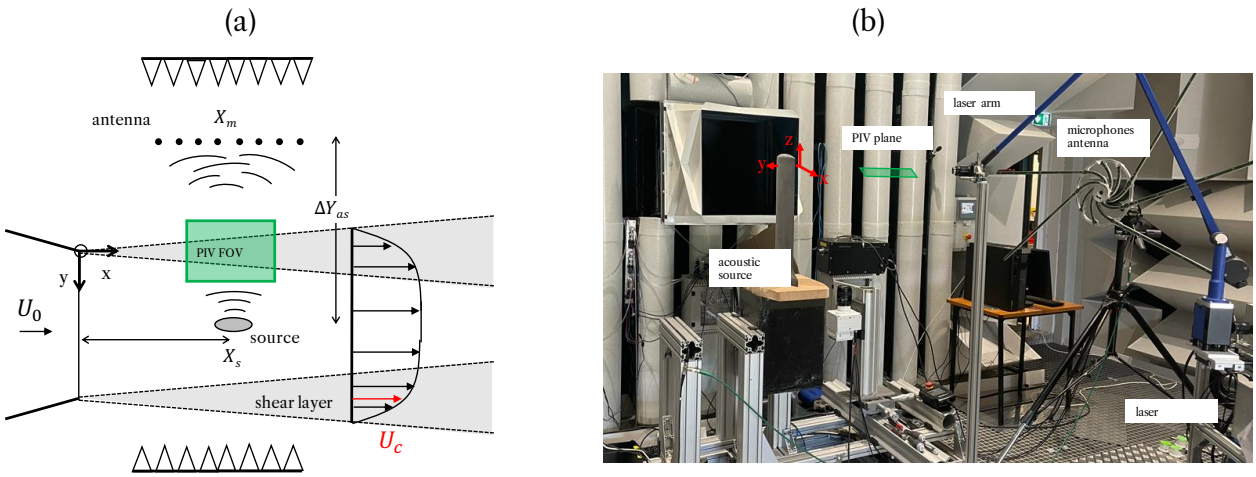

Figure 1. (a) Schematic of the experimental setup, (dimensions not in scale), (b) photos of the experimental setup.

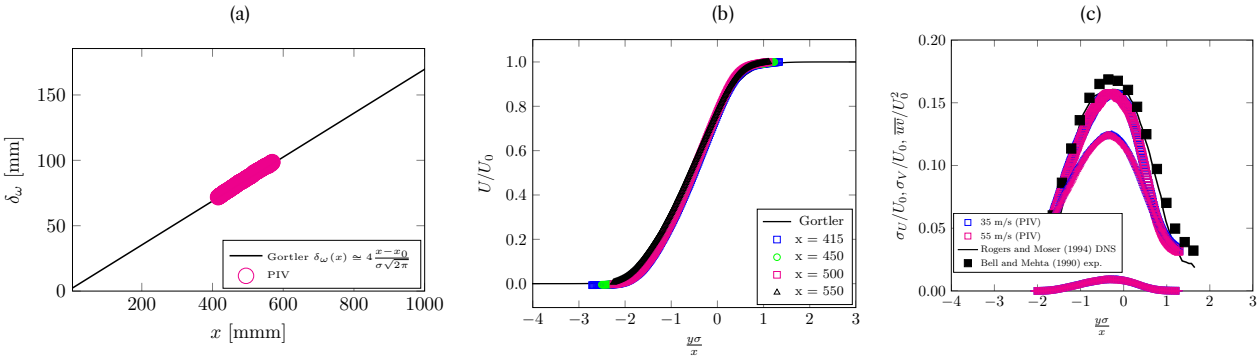

Figure 2. Linear growth of the vorticity thickness (a), collapse of the shear layer mean velocity profiles at different streamwise locations for 55 m/s (b), collapse of standard deviation of the U and V component and Reynolds shear stress at the two freestream velocities compared with Bell & Mehta (1990) and Rogers & Moser (1994) (c).

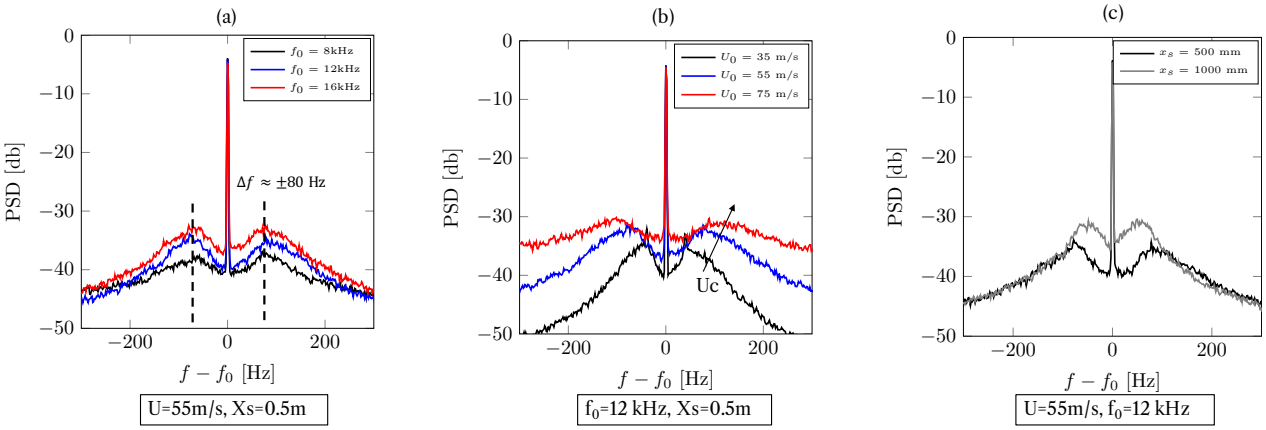

Figure 3. PSD for three different source frequencies for the microphone at $x_m = x_s$ (a) effect of source frequency at a U_0 =55 m/s and, (b) effect of the free-stream velocity U_0 at f_0 =16 kHz, (c) effect of the measurement location x_s at U_0 =55 m/s and f_0 =12 kHz.

f_1 and f_2 and a non-linear transfer of energy to the frequency $f_1 \pm f_2$.

The bicoherence spectrograms are reported in figure 4 for f_0 = 12 kHz at 35 and 75 m/s. As found by Bennaceur *et al.* (2016), high level of bicoherence are found in correspondence of the intersection of the frequencies f_1 =12 kHz and f_2 = 50 (U_0 =35 m/s) and 100 Hz (U_0 =35 m/s), frequencies that corresponds to the sidelobes of the PSD at 35 m/s and 75 m/s. This demonstrates a strong non-linear interaction between a characteristic low frequency of the shear layer and the tone frequency and the depletion of the energy of the carrier frequency into the two side-lobes.

3.3 Spectral Proper orthogonal decomposition

To further investigate the low-frequency coherent motion of the shear layer that interacts non-linearly with the acoustic

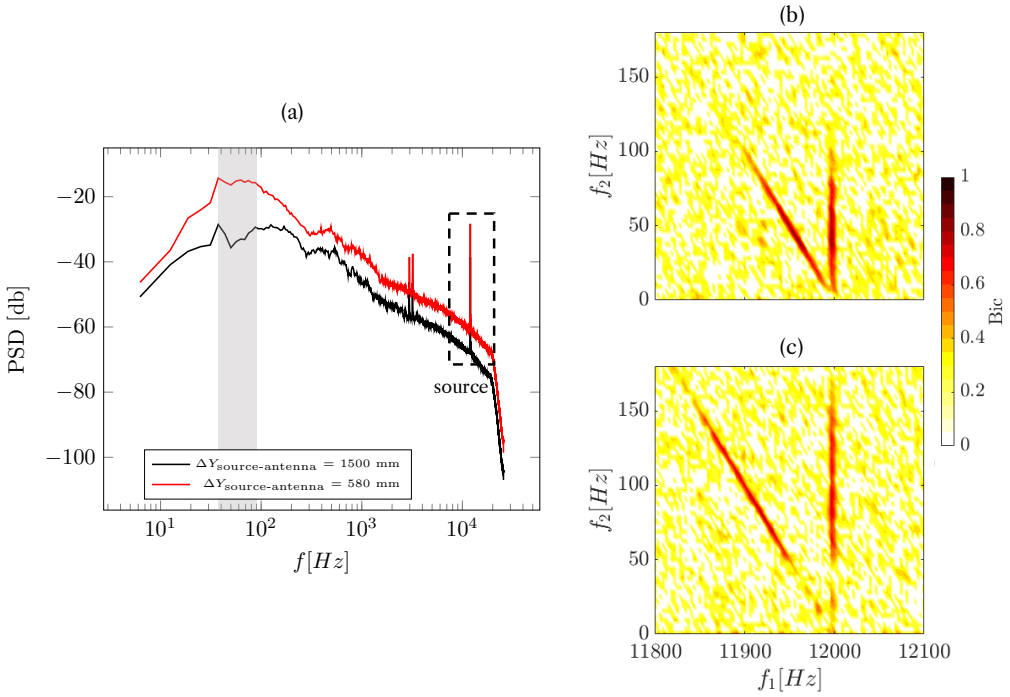

Figure 4. PSD of the signal at $x_m = x_s$, f_0 =12 kHz at 75 m/s full spectrum, effect of source-antenna distance (a), bicoherence spectrogram of the signal at $x_m = x_s$, f_0 =12 kHz, (b) 35 m/s, (c) 75 m/s.

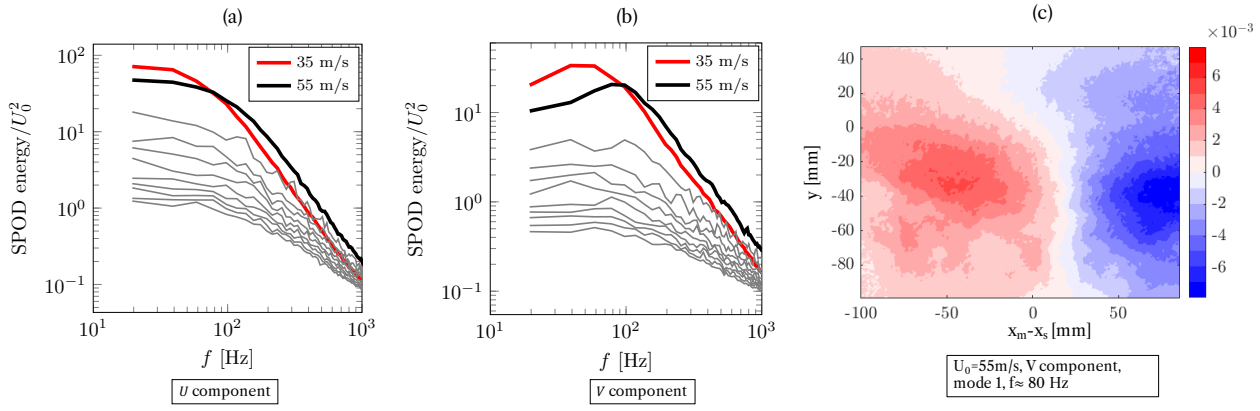

Figure 5. SPOD spectra for 35 m/s (a) and 55 m/s (b), only the ten most energetic modes are displayed, thick lines represent the leading mode (averaged on all the RUNS); snapshot of the leading sPOD mode (30% total energy) at the peak frequency for 55 m/s (c).

transmission, the spectral Proper Orthogonal Decomposition (sPOD), described by Towne *et al.* (2018), is applied to the streamwise and spanwise velocity component of the PIV data-set. The data-set is divided in 37 Hamming windows of 256 snapshots with 50% overlap. As depicted in figure 5(a) and (b), for both velocity components the first mode is dominant, however, for the spanwise component the spectrum shows a lobe centred in correspondence with the frequencies of haystacking for both 35 and 55 m/s. The contour of the mode is reported in figure 5(c) for 55 m/s and represents oriented velocity pattern in the spanwise field as depicted also in figure 6 where the spanwise velocity field at 55 m/s is reconstructed using the first SPOD mode and a frequency band centred at the peak frequency. It is worth noting that the frequency of side-bands, bicoherence and SPOD spectrum peak corresponds to a Strouhal number (obtained using the vorticity thickness and the convection velocity) approximately equal to 0.25. This Strouhal number is very close to the one of vortex shedding, suggesting, as proposed by Brown & Roshko (1974), that the coherent spanwise velocity pattern is reminiscent of the two dimensional roller forming due to the instability of a laminar shear layer in the pre-transition regime.

3.4 Flow feature time delay correlation

The oriented and coherent spanwise velocity pattern shown in figure 6 can interfere with the acoustic transmission as it is almost parallel to the acoustic wave-vector. A positive instantaneous spanwise velocity should correspond to a positive time delay of the acoustic wave and a negative spanwise velocity should correspond to a negative time delay. For each snapshot, an indicator of the instantaneous velocity is chosen by averaging the velocity inside a certain region centred with the streamwise position of the microphone aligned with the source.

The time delay due to the acoustic transmission through the shear layer is computed from the phase difference between the reference microphone installed in the source case and the

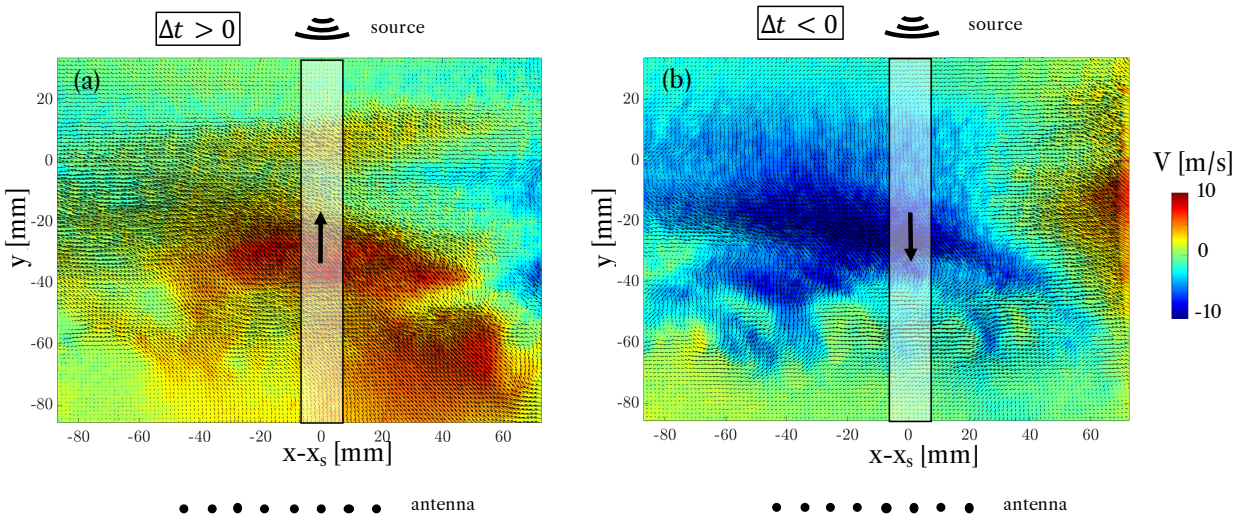

Figure 6. Spanwise velocity field at 55 m/s reconstructed using the first SPOD mode in a frequency interval of 30-100 Hz (a) oriented positive velocity (b) oriented negative velocity.

microphone on the antenna knowing the distance between the source and the antenna. Further details on the time delay evaluation can be found in Sijtsma *et al.* (2014). As depicted in figure 7 the time delay is negligible when the free-stream velocity is zero and increases when increasing the free-stream velocity. The time delay is calculated on the acoustic signal synced with the PIV acquisition.

When plotting the normalised indicator and time delay on top of each other (figure 7 (c)) one can see how the signals collapse remarkably well. The correlation between the time delay and the streamwise and spanwise component is reported in figure 8. As depicted in the figure, a correlation as high as 0.5 is found for the spanwise component while the correlation is negligible for the streamwise component. What needs to be underlined, and can be considered a validation of the current result, is that the peak of correlation (figure 8 (b)) is associated with a time that corresponds exactly to time the acoustic waves take to reach the antenna from the PIV measurement plane. Similar results are found when the spanwise field is not filtered, the main difference is that the indicator is less accurate due to the small scales and higher frequency turbulence.

4 Conclusions

We performed for the first time synced PIV and microphones measurements. The bicoherence results revealed that the haystacking is due to a non-linear interaction between the acoustic carrier tone and a low frequency feature of the turbulent shear layer. The low frequency feature is a shedding-like oriented motion of the spanwise velocity component, with a characteristic Strouhal number of 0.25 which is documented both in the SPOD spectrum and in the side-lobes of the PSD of the acoustic signal. The synced PIV-microphone results corroborate the theoretical derivation proposed by Sijtsma *et al.* (2014) that links the haystacking with the acoustic transmission delay/anticipation due to the turbulent field. The time delay/anticipation is indeed correlated with the turbulent shear layer instantaneous spanwise velocity pattern.

REFERENCES

Bell, James H. & Mehta, Rabindra D. 1990 Development of a two-stream mixing layer from tripped and untripped boundary layers. *AIAA Journal* **28** (12), 2034–2042.

Bennaceur, Iannis, Mincu, Daniel C., Mary, Ivan, Terracol, Marc, Larchevêque, Lionel & Pierre, Dupont 2016 Physical Analysis of Acoustic Scattering by a Turbulent Shear Layer using Numerical Simulation. In *22nd AIAA/CEAS Aeroacoustics Conference*. Lyon, France: American Institute of Aeronautics and Astronautics.

Brown, Garry L. & Roshko, Anatol 1974 On density effects and large structure in turbulent mixing layers. *Journal of Fluid Mechanics* **64** (4), 775–816.

Candel, S., Guedel, A. & Julienne, A. 1976*a* Résultats préliminaires sur la diffusion d'une onde acoustique par écoulement turbulent. *Le Journal de Physique Colloques* **37** (C1), C1–153–C1–160.

Candel, Sebastien, Julienne, A. & Guedel, A. 1975 Refraction and scattering of sound in an open wind tunnel flow. In *ICIASF'75; 6th International Congress on Instrumentation in Aerospace Simulation Facilities*, pp. 288–300.

Candel, S., Julliand, M. & Julienne, A. 1976*b* Shielding and scattering by a jet flow. In *3rd Aeroacoustics Conference*. Palo Alto,CA,U.S.A.: American Institute of Aeronautics and Astronautics.

Clair, Vincent & Gabard, Gwénaël 2018 Spectral broadening of acoustic waves by convected vortices. *Journal of Fluid Mechanics* **841**, 50–80.

Ewert, Roland, Kornow, Oliver, Delfs, Jan, Roeber, Thomas & Rose, Marco 2009 A CAA Based Approach to Tone Haystacking. In *15th AIAA/CEAS Aeroacoustics Conference (30th AIAA Aeroacoustics Conference)*. Miami, Florida: American Institute of Aeronautics and Astronautics.

Görtler, H. 1942 Berechnung von Aufgaben der freien Turbulenz auf Grund eines neuen Näherungsansatzes . *ZAMM - Zeitschrift für Angewandte Mathematik und Mechanik* **22** (5), 244–254.

Kim, Young C. & Powers, Edward J. 1979 Digital Bispectral Analysis and Its Applications to Nonlinear Wave Interactions. *IEEE Transactions on Plasma Science* **7** (2), 120–131.

Kraichnan, Robert H. 1953 The Scattering of Sound in a Turbulent Medium. *The Journal of the Acoustical Society of America* **25** (6), 1096–1104.

Kroeber, Stefan, Hellmold, Marius & Koop, Lars 2013 Ex-

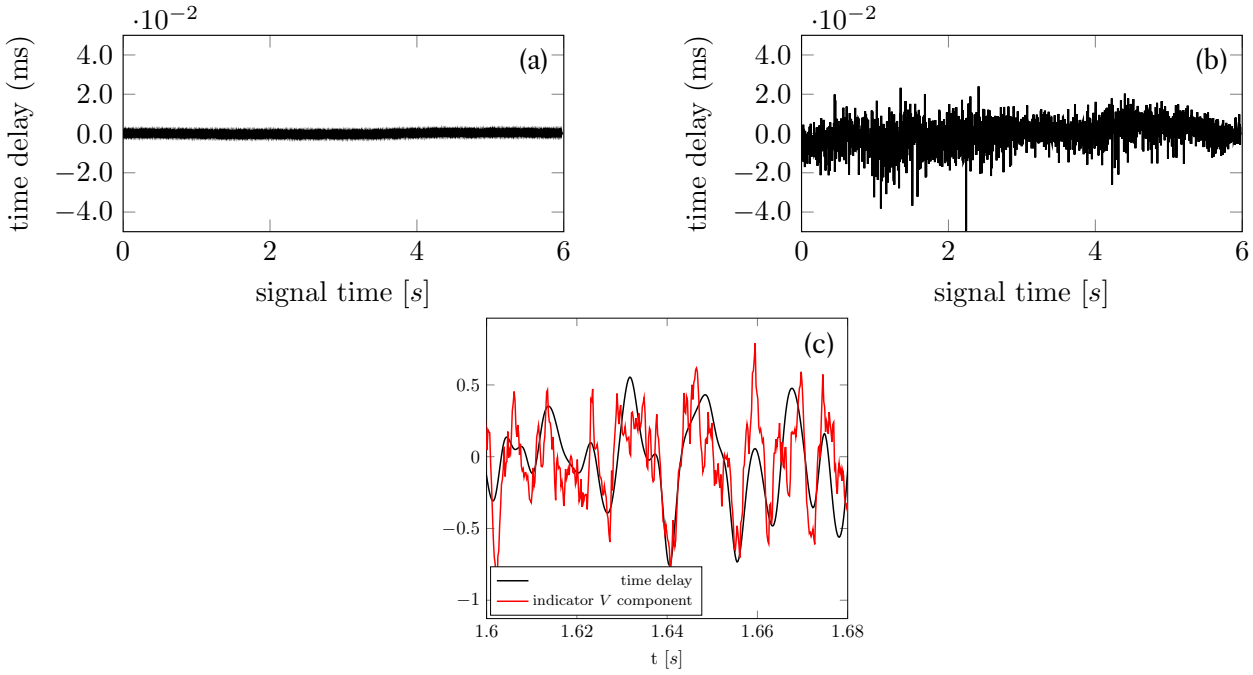

Figure 7. Time delay calculated with the phase shift with respect to the reference microphone in the source Sijtsma *et al.* (2014), (a) no flow and (b) 55 m/s, (c) normalised time delay for 55 m/s with superimposed the spanwise velocity indicator.

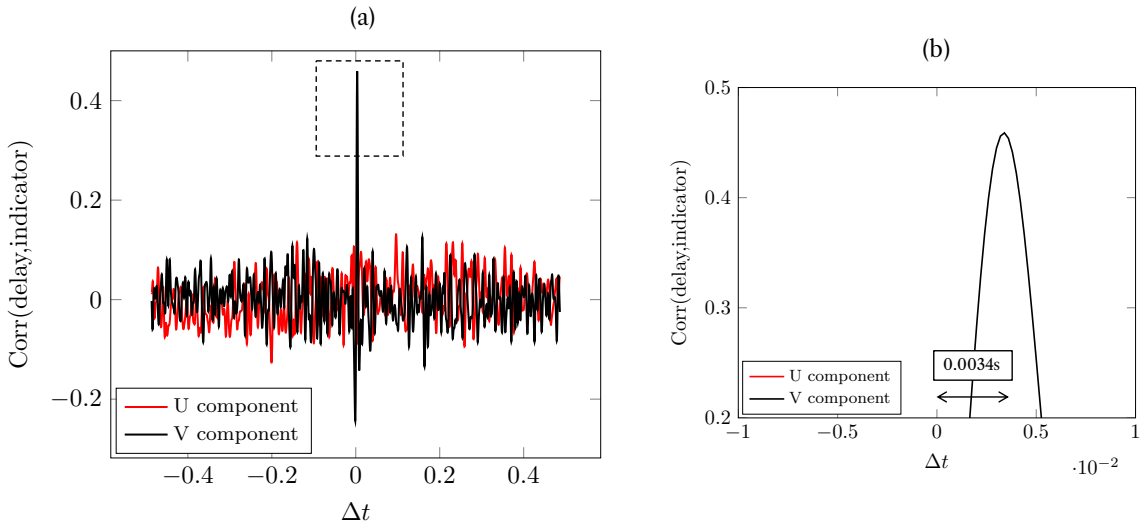

Figure 8. Correlation coefficient between the velocity indicator and the time delay both normalised with respect to the maximum value for the streamwise and the spanwise component (a), zoom on the peak of the spanwise component (b).

perimental Investigation of Spectral Broadening of Sound Waves by Wind Tunnel Shear Layers. In *19th AIAA/CEAS Aeroacoustics Conference*. Berlin, Germany: American Institute of Aeronautics and Astronautics.

Lighthill, M. J. 1953 On the energy scattered from the interaction of turbulence with sound or shock waves. *Mathematical Proceedings of the Cambridge Philosophical Society* **49** (3), 531–551.

McAlpine, A., Powles, C.J. & Tester, B.J. 2013 A weak-scattering model for turbine-tone haystacking. *Journal of Sound and Vibration* **332** (16), 3806–3831.

Michaelis, Dirk, Neal, Douglas R & Wieneke, Bernhard 2016 Peak-locking reduction for particle image velocimetry. *Measurement Science and Technology* **27** (10), 104005.

Rogers, Michael M. & Moser, Robert D. 1994 Direct simulation of a self-similar turbulent mixing layer. *Physics of Fluids* **6** (2), 903–923.

Sijtsma, Pieter 2008 Acoustic array corrections for coherence loss due to the wind tunnel shear layer. In *Berlin Beamforming Conference (BeBeC)*.

Sijtsma, Pieter, Oerlemans, Stefan, Tibbe, Tim G., Berkefeld, Tobias & Spehr, Carsten 2014 Spectral Broadening by Shear Layers of Open Jet Wind Tunnels. In *20th AIAA/CEAS Aeroacoustics Conference*. Atlanta, GA: American Institute of Aeronautics and Astronautics.

Towne, Aaron, Schmidt, Oliver T. & Colonius, Tim 2018 Spectral proper orthogonal decomposition and its relationship to dynamic mode decomposition and resolvent analysis. *Journal of Fluid Mechanics* **847**, 821–867.